Journal of Photochemistry and Photobiology 14 (2023) 100171

Contents lists available at ScienceDirect

Journal of Photochemistry and Photobiology

journal homepage: www.sciencedirect.com/journal/journal-of-photochemistry-and-photobiology

ZnO UV sensor photoresponse enhancement by coating method optimization

Mindaugas Ilickas [a], Mantas Marčinskas [a,b], Domantas Peckus [a], Rasa Mardosaitė [a,c], Brigita Abakevičienė [a,c], Tomas Tamulevičius [a,c], Simas Račkauskas [a,c,*]

[a] Institute of Materials Science of Kaunas University of Technology, K. Baršausko St. 59, LT-51423 Kaunas, Lithuania
[b] Department of Organic Chemistry, Kaunas University of Technology, Radvilėnų St. 19, LT-50254, Kaunas, Lithuania
[c] Department of Physics, Kaunas University of Technology, Studentų St. 50, LT-51368 Kaunas, Lithuania

ARTICLE INFO

Keywords:
ZnO tetrapods
UV sensor
Coating methods
Photoresponse
Inter-electrode gap

ABSTRACT

Modern high-performance photodetector research is driven by the need to simultaneously improve multiple parameters, but also fit the decreasing size of electronics and maintain low production price. Here, we demonstrated how our synthesized ZnO tetrapod (ZnO-T) nanostructure was deposited on electrodes with variating gap by four coating methods including drop casting, microdrop casting, spray coating and slot-die coating with the same thickness. Optimizing the inter-electrode gap and coating method the record I_{UV}/I_{Dark} ratio per unit area value of 8.73×10^6 was obtained. The fastest rise time 0.78 s and fastest decay time 0.94 s were obtained by slot-die coated sensors. High photoresponse of ZnO-Ts, the inter-electrode gap size influences formation of ZnO-T microstructure during coating process and morphology influence on photoresponse was explained. We demonstrate that even with the same optimized ZnO-T nanostructures photoresponse can be improved by 2 orders of magnitude. Our work shows the importance of coating morphology and inter-electrode gap optimization.

Introduction

Zinc oxide at ambient temperature is an II-VI semiconductor with a considerable excitation binding energy of 60 meV and a broad bandgap (~3.37 eV) [1]. Due to innovative optical and electrical characteristics and prospective applications in the realms of photonic and electronic devices, the interest in nanoscale ZnO materials with specific morphologies have recently increased [1].

UV sensors based on ZnO nanostructures have been investigated because of the large surface-to-volume ratio which can improve the devices' performance [2]. In comparison to bulk and thin film materials, one-dimensional (1D) structures, such as nanowires have a substantially higher surface area per unit volume and a peculiar electron transfer characteristic. As a result, nanowire based chemosensors, especially semiconducting metal oxide ones are often applied in sensing and photodetection [3]. ZnO tetrapod is the structure, consisting of 4 connected legs linked to a central core. ZnO-T legs have the like nanowire properties and the advantage, that compact aggregation is intrinsically hindered [4–6]. ZnO-T nanostructures in general are promising for applications in optoelectronics [7,8] and specifically for UV photodetectors [9–11].

In principle ZnO nanoparticle UV sensor fabrication involves creating a gap between two electrically conductive contacts and filling it with ZnO nanomaterial. In contrast to classical methods of ZnO sputtering [12] which is expensive and pose other limitations, more straightforward methods include spray coating [13], dip coating [14], printing [15], spin coating [16] or simply drop casting [17], such methods have more potential for application in flexible electronics [18, 19]. The spray coating utilizes a spray gun that forms the dispersion of the nanoparticle suspension into minuscule droplets with sizes <10 μm [20], then scattered on desired surfaces [21]. As the solvent evaporates from the substrate, nanoparticle films develop. Spray coating is generally unaffected by the surface morphology, may be applied to a variety of substrates and is not limited by substrate size [22]. Slot-die coaters employ the liquid meniscus and the moving substrate, enabling the use of low viscosity nanoparticle suspensions. The wet layer forming during coating process allows for spontaneous drying, which reduces production time and waste of solution [22]. Drop casting is probably the most

* Corresponding author.
E-mail address: simas.rackauskas@ktu.lt (S. Račkauskas).

https://doi.org/10.1016/j.jpap.2023.100171
Received 14 November 2022; Received in revised form 17 February 2023; Accepted 26 February 2023
Available online 3 March 2023

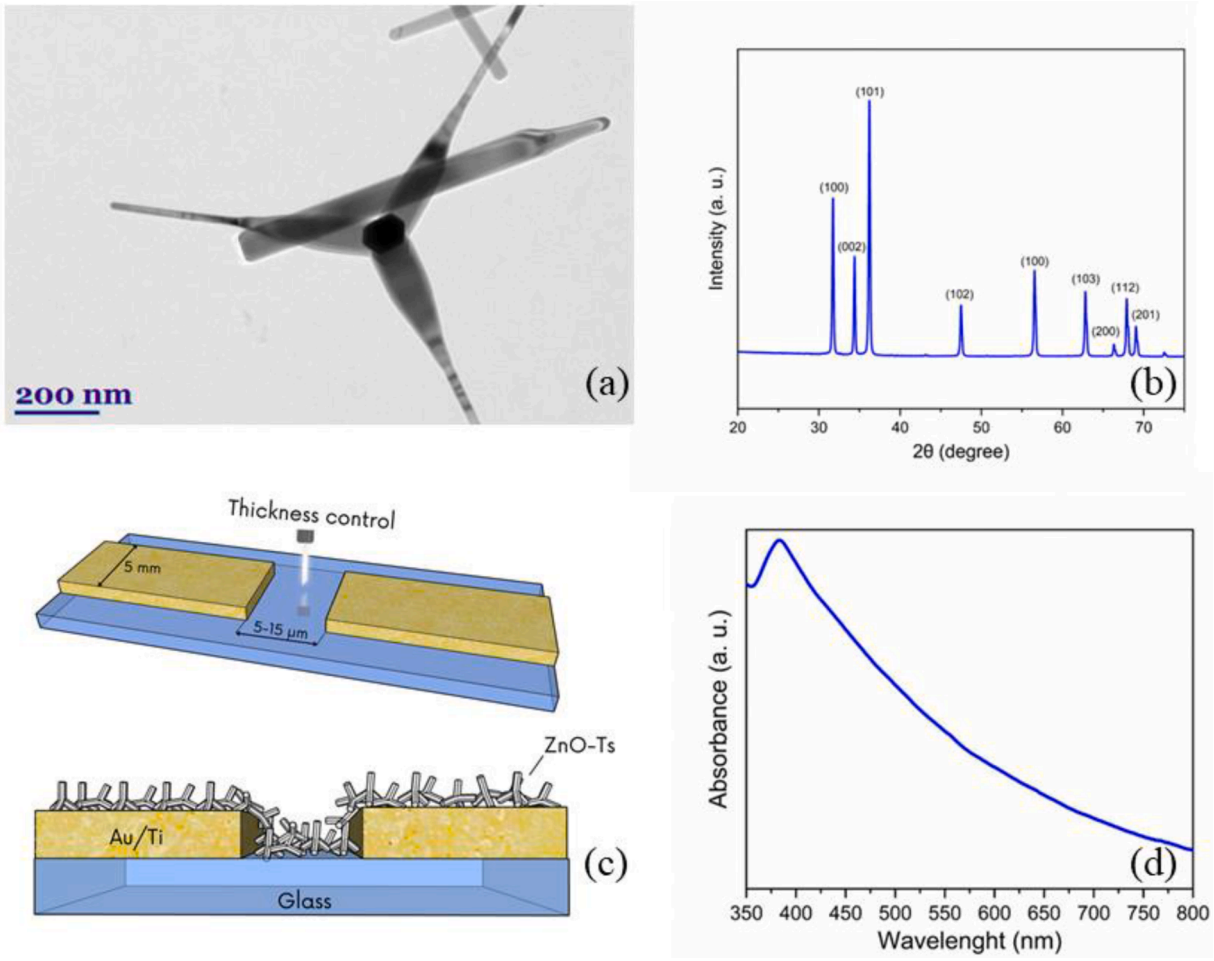

Fig. 1. ZnO tetrapod (ZnO-T) characterization: (a) TEM image of ZnO-T structure (b) XRD spectrum; (c) sensor preparation scheme where vacuum deposited film is locally removed by the fs-laser ablation forming a defined gap between two electrodes followed by the deposition of the ZnO-Ts from the suspension; (d) UV–Vis's absorption spectrum.

basic approach [17] that is commonly used for sensor preparation in laboratories [23], however, some other techniques e.g., printing [15] have similar features. The process involves simply placing a droplet of nanoparticle suspension on the substrate, the film forms after solvent dry-out.

Most common techniques for nanoparticle film formation use suspension deposition on the substrate. Evaporation of the solvent during coating induces complicated processes, the morphologies of the formed coatings are influenced by macroscopic effects such as internal flow structure [24] and contact line dynamics [25], as well as microscopic effects such as particle-interface/particle-particle interaction [26]. The most well-known deposit patterns are coffee-ring, uniform, dot-like, and stick-slip.

The coffee-ring pattern forms during a droplet with nanoparticles complete evaporation on a solid surface, leaving behind a ring-like deposit. The outward capillary flow is responsible for the formation of an aggregated particle ring, which settles at the circumference of the droplet after complete evaporation [27]. Coffee rings do not form for small scale extinctive microdroplets, for a particle size of 100 nm, the diameter of the droplet resulting in the coffee-ring pattern must be larger than 10 μm [28].

The ratio of current under UV illumination (I_{UV}) to initial current in dark (I_{Dark}), commonly known as photo to dark current ratio (I_{UV}/I_{Dark}) is one of the key figures of merit for photodetectors [10]. To improve ZnO UV sensors performance several routes are employed: various ZnO structures, such as nanopowder [29], nanowires [30], tetrapods [4] or other nanostructures [31] are used. Optimization of ZnO nanostructure diameter and porosity [10] or other morphological parameters [6], lead to better oxygen and electrical transport. Alternatively, to enhance the optoelectrical properties of ZnO nanostructures, doping with Al, Ga, Sb, Ag, Cu, As, Mo or other elements is used [32,33]. UV sensor performance can be increased by supplemental materials on electrode contacts such as high work function metals Au [34], Pt [35] of carbon nanomaterials such as graphene [36] and carbon nanotubes [37] or Schottky barriers [19,38,39] can be employed. However, the UV sensor performance is commonly measured on the interdigitated electrodes [4,10,19] and the influence of the inter-electrode gap is mostly disregarded. Moreover, the influence of different coating methods for the coating of the same nanostructures is disregarded, detailed studies on the influence of nanoparticle coating methods on the photoresponse are needed.

In this work we investigated the influence of coating methods and inter-electrode gap on the photoresponse for the ZnO-T sensor. Four coating methods including drop casting, microdrop casting, spray coating and slot-die coating were employed to deposit same thickness of ZnO-T on the electrodes with variating gap, forming UV sensors. Controlling the amount of deposited ZnO-T and using the same structure in all experiments we were able to reach several orders of magnitude improvement on photoresponse. This improvement allowed us to reach the record value of I_{UV}/I_{Dark} ratio per area adhering to the global trend in miniaturization of electronics. This work demonstrates the importance of the inter-electrode parameter and morphology control and opens the new direction for ZnO, or other semiconductor nanoparticle based

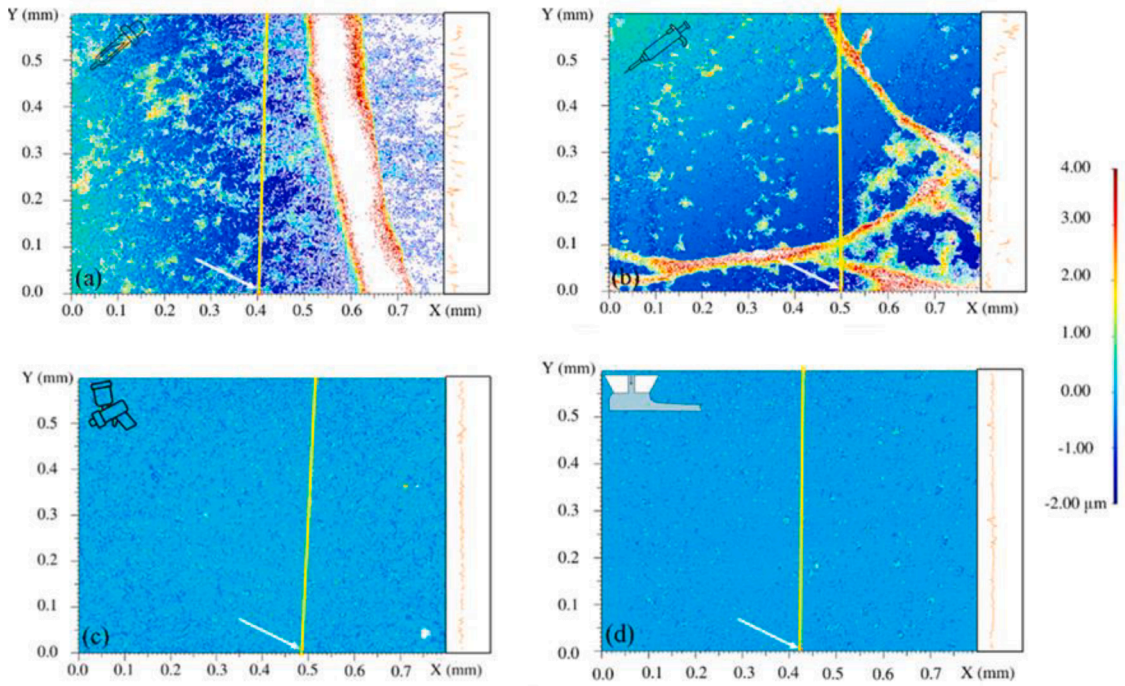

Fig. 2. Profilograms of ZnO-T UV sensors, coated by: (a) drop casting method, 10 µm inter-electrode gap; (b) microdrop casting method, 15 µm inter-electrode gap; (c) spray coating method, 5 µm inter-electrode gap; (d) slot-die coating method, 10 µm inter-electrode gap. An arrow marks the inter-electrode gap (yellow line), height profile of the gap is shown on the right.

chemoresistive sensor improvement.

Materials and methods

UV Sensor preparation

ZnO-Ts were synthesized using a rapid oxidation (combustion) approach [40], in which micron sized Zn particles (Sigma-Aldrich, product no. 96454) were combusted in the surrounding air atmosphere with additionally superheated water steam supplied throughout the synthesis process. The particles, collected on the filter (Whatman, pore size 0.45 µm, diameter 25 mm) downstream were suspended in ethanol (Eurochemicals, ≥ 99%) and centrifuged at 1000 rpm for 15 min to obtain the final fraction, which was dried and used in this work.

For all coating methods ZnO-T solutions were prepared as follows: 5 mg/ml ZnO-Ts in isopropyl alcohol (2-propanol) (Eurochemicals, ≥ 99%) were prepared, the solutions were stirred for 15 min in an ultrasonic bath to suspend the particles. ZnO-Ts suspension was coated on 2 electrodes with an inter-electrode gap of 5 µm, forming a UV sensor (Fig. 1c). Electrodes were deposited by sputtering, substrate – glass, electrode thickness – 50 nm Ti underlayer and 150 nm Au on top. Inter-electrode gaps – 5 µm, 10 µm and 15 µm, where made by femtosecond laser cutting employing second harmonic of the Yb:KGW laser (Pharos, Light Conversion) and translating the sample with respect to 0.42 NA microscope objective. To control the coating thickness, after each coating round an optical thickness of dried film was determined by the custom build UV absorption meter registering relative change in absorption at the central wavelength of 365 nm. For all experiments the optical thickness was kept constant at 50% film transmission value, which should eliminate shadowing of thicker film patches and guarantee optimal conditions.

In this work four different ZnO-T coating deposition methods were used: 1) drop casting method with a pipette (drop volume 0.1 ml, drop mass 73 mg), 2) microdrop casting method with a micropipette (drop volume 10 µl, drop mass 8.5 mg), 3) spray coating method (pressure 1.5 bar, distance between the nozzle and the sensor 15 cm), 4) slot-die coating (Ossila, coating speed 10.3 mm/s, dispense rate 10.3 µL/s, substrate temperature 80 °C). In all experiments, the room temperature was 23±1 °C and the relative humidity 25±1%.

Materials characterization

The optical properties of ZnO coatings were investigated using the 172–1100 nm spectral range and resolution 1.4 nm UV–VIS-NIR spectrometer (AvaSpec-2048, Avantes) and a combined deuterium and halogen light source. The structural characterization of ZnO powders was evaluated with a D8 Discover X-ray diffractometer (Bruker AXS GmbH) with a Cu Kα ($\lambda = 1.5418$ Å) radiation source and a parallel beam geometry with a 60 mm Göbel mirror. Peak intensities were scanned throughout a 20 to 75° range (coupled $\theta-2\theta$ scans) using a step size of 0.02° The International centre for Diffraction Data (ICDD) database was used to compare XRD patterns and identify the ZnO phase. The surface texture was investigated using the 0.02 µm resolution, 100 µm measurement range, non-contact white-light interferometer WS 1 (MarSurf) and scanning electron microscope (SEM) Quanta 200 FEG (FEI). Structural high-resolution TEM measurements were carried out by Tecnai G2 F20 X-TWIN TEM (FEI) operating at 200 kV. Electrical measurements of UV sensors were performed on a probe stage using A KEITHLEY 6487 picoammeter and LINKAM HFS600E-PB4 with UV source ProLight Opto PB2D-3JLA-GS LED. The response speed was defined as the rise time (the time taken by the sensor to reach 90% of the maximum photocurrent) and the decay time (the time taken to get 10% of the maximum photocurrent).

Results and discussion

Structural and morphological investigation

TEM investigation of ZnO-T (Fig. 1a) reveals the tetrapodal structure of the ZnO, with 4 legs connected in one point. Lose nanowires, not connected into tetrapodal structures are also apparent in the mixture and can be caused by breaking of tetrapod structures after centrifuging.

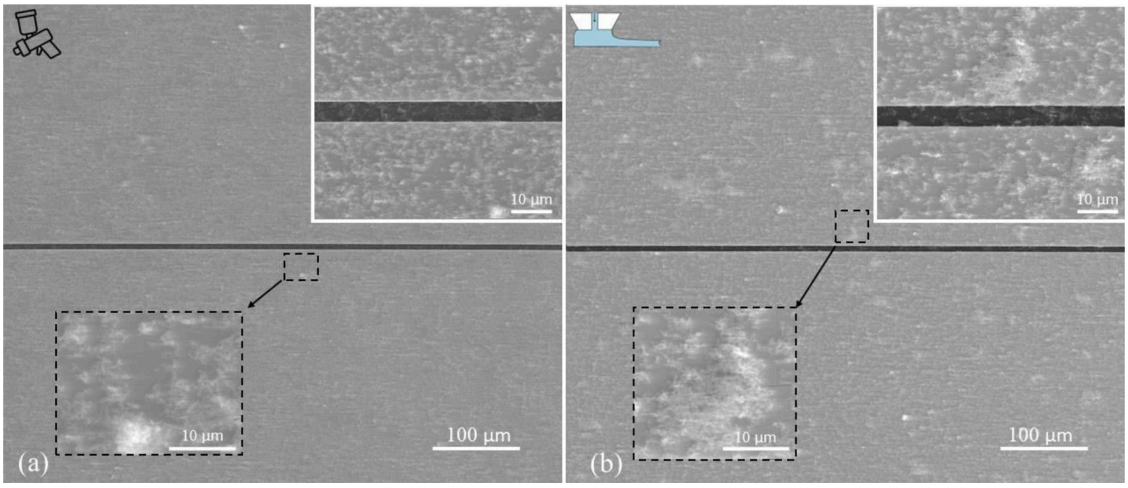

Fig. 3. SEM images of UV sensor made from ZnO-Ts coated by (a) spray coating method and (b) slot-die coating highlighting coating qualities (insets) next to the 5 μm inter-electrode gap.

Diameter of the legs are in the range of 30–80 nm, and the length is 200 – 500 nm.

The X-ray diffraction graph of the ZnO sample is illustrated in Fig. 1 (b). All XRD peaks were indexed by the hexagonal wurtzite crystal structure [41] of ZnO with the most preferred orientations (100), (002), and (101) according to the JCPDS database (card. No. 00–036–1451), their most robust line corresponding to the (101) plane. No peaks of any other phase were observed, confirming the absence of impurities in the ZnO powders. The peaks of ZnO diffractogram at 2θ values 34.4°, 37.8°, 36.2°, 47.5°, 56.6°, 62.8°, 66.3°, 67.9°, 69.0°, 72.5° could be assigned to (100), (002), (101), (102), (100), (103), (200), (112), and (201), planes respectively. The average crystallite size (D_{hkl}) of the nanostructures was calculated based on the Debye-Scherer equation [42]:

$$D = \frac{K_{hkl}\lambda}{\beta_{hkl} cos\theta} \quad (1)$$

where λ – the length of Cu Kα radiation (1.54056 Å), θ – the diffraction angle, β_{hkl} – full width at half maximum (FWHM) in radians, k – a constant (0.94), D_{hkl} – the size of the crystallites, nm.

The average crystallite size of the ZnO nanoparticles estimated by Eq. (1) was found to be 42.4 nm.

Fig. 1(d) shows UV–vis absorption spectrum of the – ZnO-Ts. Our synthesized nanoparticles (ZnO-Ts) have an intensity maximum at λ_{max}=375.98 nm. The spectrum shows a characteristic absorption peak of ZnO-Ts and other ZnO nanoparticles seen in our earlier work [43]. The peak is addressed to the intrinsic band gap absorption of ZnO in connection to the electron transitions from the valence band to the conduction band ($O_{2p} \rightarrow Zn_{3d}$) [44].

Surface morphology of the coated UV sensors which showed the best I_{UV}/I_{Dark} ratio is depicted in Fig. 2. A yellow vertical line indicated by an arrow in the center of the figures marks the inter-electrode gap, and the height profile from this line can be followed by the color-coded height information with a scale on the right of the figure.

It can be noticed that using the drop casting method, large nanoparticle agglomerates called coffee-rings [45], with a ring line thickness of ~ 100 μm are formed, and the white color indicates that the selected scale (−2.00 – 4.00 μm) is exceeded (Fig. 2a). The height profile at the inter-electrode gap (Fig. 2a right), shows the variating coating thickness drop casting up to 1.5 μm, an uneven character of coating at the gap can be noticed. Microdrop casting coating method produces narrower rings drop casting with the ring line thickness of ~ 50–80 μm (Fig. 2b), however, height profile at the inter-electrode gap shows a more even coating, except for places where the coffee-rings cross the gap, increasing the coating thickness up to 3.0 μm. Spray coating (Fig. 2c)

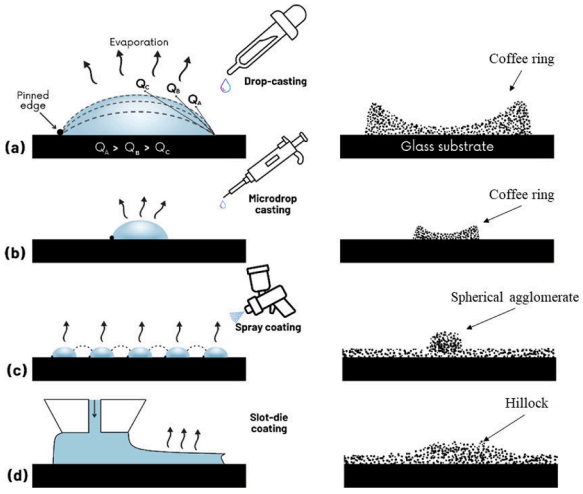

Fig. 4. Schematics of suspension with nanoparticles evaporation (on the left) and formed nanoparticle coatings for coating methods: (a) drop casting; (b) microdrop casting; (c) spray coating; (d) slot-die coating.

and slot-die coating (Fig. 2d) methods, result in a much more uniform and smoother coating, there are no significant fluctuations in height profile on the gap. However, in case of spray coating some nanoparticle aggregations are observed on the surface, moreover they are larger in size, compared to the surface prepared by slot-die coating method. The slot-die coating method with ZnO nanoparticles yields the most dense and thinnest coating and reaches up to 1 μm at the inter-electrode gap. Despite thinner thickness the slot-die coating still demonstrates the same optical thickness related to the optical attenuation and therefore mass deposition on the substrate.

ZnO-T films prepared by slot-die and spray coating methods appear similar in profilometer, therefore SEM was employed to further investigate the morphology (Fig. 3). Both coatings consist of the small groups of nanoparticles, evenly distributed all over the surface and some larger agglomerates. Spray coated films have some spherical aggregations of 3–5 μm size (Fig. 3a marked with square and magnified) on the surface. Films coated by slot-die method apart from spherical aggregates form hillocks of 10–50 μm wide, which appear less dense than spherical aggregations.

Based on the SEM and optical profilometer analysis the main characteristics of the coating formation by four different deposition methods were proposed (Fig. 4). Drops with nanoparticle suspension, deposited

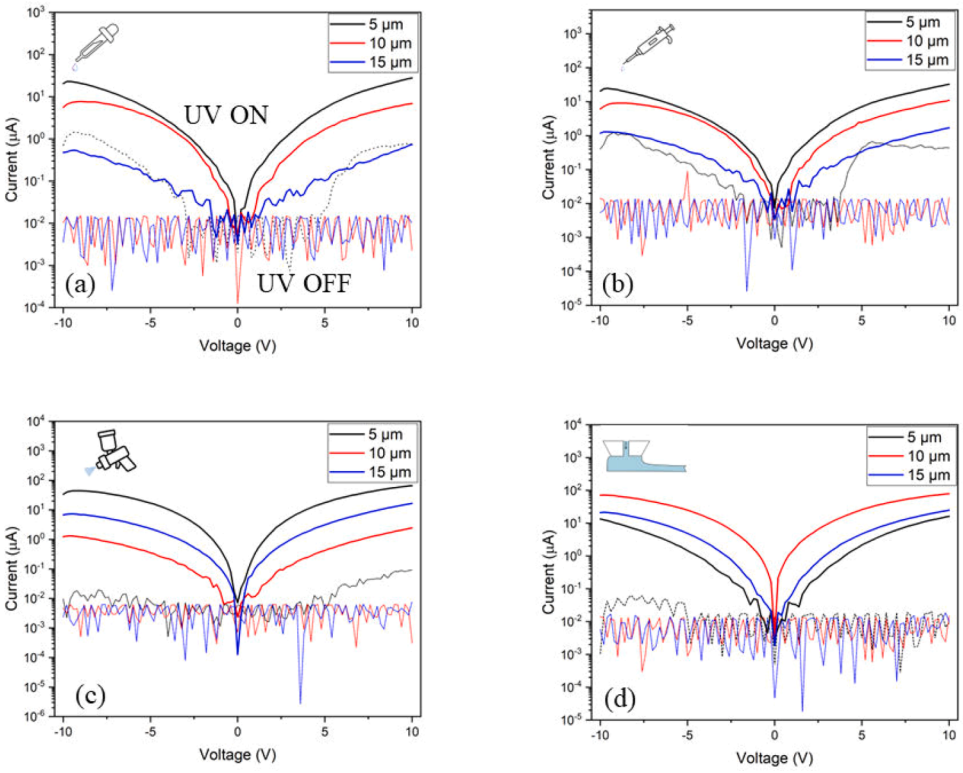

Fig. 5. Current-voltage characteristics of UV sensors prepared by coating methods: (a) drop casting; (b) microdrop casting; (c) spray coating; (d) slot-die coating. A dashed line indicates measurements in dark, solid line under UV illumination.

on a substrate develop to the coating through the evaporation, which induce complex inner flow phenomena and cause the formation of coffee-ring patterns [27]. Drop evaporation on the substrate involves the pinning of the edge and receding of the contact angle from Q_A to Q_C (Fig. 4. a), the inner flow occurring due to evaporation rate gradient transports the nanoparticles to the pinned edges and forms ring-like

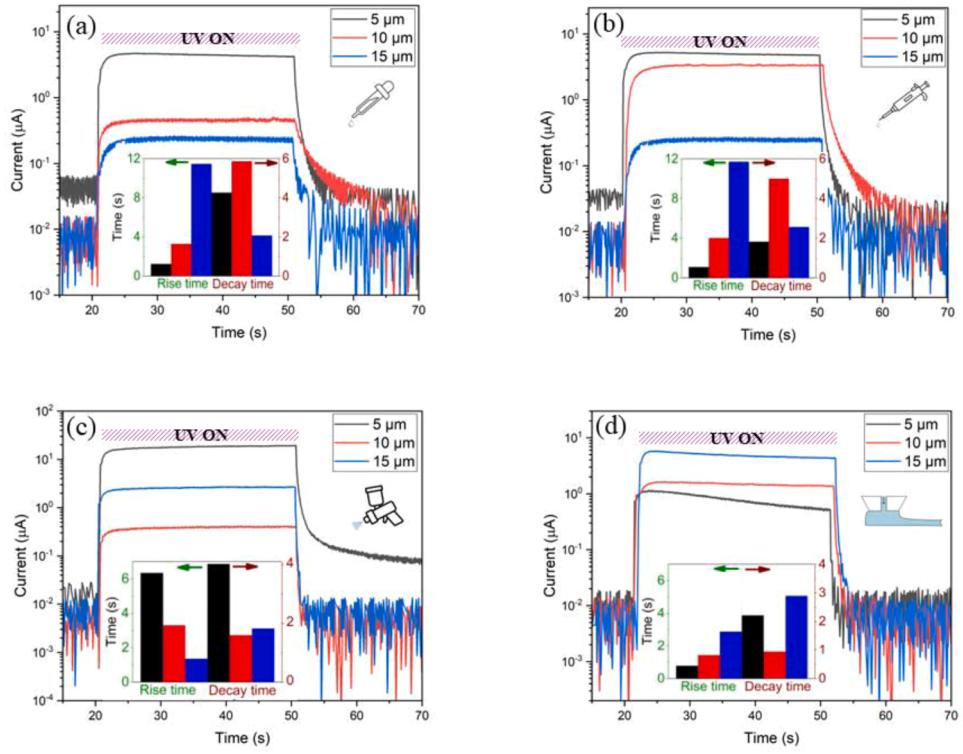

Fig. 6. Dynamic response to a $\tau = 30$s UV pulse for the sensors coated by (a) drop casting; (b) microdrop casting; (c) spray coating; (d) slot-die coating. The inset shows rise and decay times.

aggregates [46,47]

The size of such rings, their height and width depend on the initial drop diameter as we can see in Fig. 3a and b (and schematically shown in Fig. 4a and b), microdrops result in more narrow coffee-rings. Drop and microdrop casting have similar pattern, with the coffee-ring in the surroundings and the more even surface with smaller agglomerations at the center. However, in case of the drop-casting coffee-rings are away from the inter-electrode gap and in microdrop casting, multiple rings are crossing the gap.

Spray coating and slot-die coating methods form an even nanoparticle film without coffee-rings. Coffee-ring pattern does not form for drops smaller than 10 μm (or 50 μm if no surfactants are used) for a suspension with particle size of 100 nm [28] since spray coating method produces droplets with mean diameter <10 μm [20], therefore spray coating method forms a uniform coating. Slot-die coating also forms even coating since drop formation is not involved in the coating process at all. Edge pinning occurs only at the beginning of deposition and the whole nanoparticle suspension supply front is dragged over the surface at a constant speed, also forming a uniform nanoparticle film after drying. Both slot die and spray coating methods form equally uniform distribution of nanoparticles over the surface, however some random aggregation of nanoparticles occur. In case of spray coating, some spherical aggregates can be observed (marked with square in Fig. 3a) which might be due to aggregation in the stock suspension used for spraying. Slot-die coating besides similar spherical aggregations, also form hillocks (marked with square in Fig. 3b), which might form during the deposition.

UV sensing performance

To compare the influence of coating method on the UV photoresponse, electrodes with gaps of 5 μm, 10 μm and 15 μm were coated employing 4 discussed methods with the same ZnO-T nanoparticles. To ensure that all methods have the same amount of deposited ZnO-Ts, coating process was proceeded until 50% absorbance was reached. Two distinct groups of coating methods demonstrating similar UV photoresponse can be distinguished: a) drop and microdrop casting; b) spray and slot-die coating.

Current-voltage (*I-V*) characteristics of the coated sensors examined after UV (λ=365 nm, $I = 0.31$ mW/cm^2) irradiation is depicted in Fig. 5. All sensors had a non-linear *I–V* characteristic due to the development of potential energy barriers between individual ZnO nanostructures and microstructures in the 3D network topologies [48]. The dark current (dashed line) is orders of magnitude lower than photocurrent (solid line) and mostly is limited by the measurement possibilities, except for the drop and microdrop casting coated sensors with 5 μm gap.

Fig. 6 shows the current-time response curves to a τ=30 s duration UV pulse. Slot-die coated sensors show best performance with I_{UV}/I_{Dark} ratio 28×10^3 (10 μm gap), spray coated sensors show almost identical I_{UV}/I_{Dark} ratio 2.2×10^3 but for smaller gap of 5 μm. Interestingly, for both coating methods inter-electrode gap change (lowering to 5 μm for slot-die and increasing to 10 μm for spray coating) lowers the I_{UV}/I_{Dark} ratio by ~20 times. Drop and microdrop casting show much lower photoresponse with the highest I_{UV}/I_{Dark} ratios of 1.0×10^3 (10 μm gap) and 1.8×10^2 (15 μm gap) for drop and microdrop casting coated sensor, respectively (Table S3 supporting information). The fastest rise time was demonstrated by the sensor prepared by the slot-die coating method (0.78 s for 5 μm gap), which was similar to the same gap sensors coated by the drop and microdrop casting method (1.09 s and 1.23 s, respectively), the slowest rise time showed the spray coated sensor (6.34 s). The fastest decay time demonstrated the sensor coated by the slot-die method (0.94 s, 15 μm gap), and the spray coated sensor (1.35 s, 15 μm gap), and the slowest decay time had the sensor coated by the spray coating method (15.98 s, 5 μm gap). We demonstrate how the coating method and inter-electrode gap optimization gives an I_{UV}/I_{Dark} ratio difference of 200 times (1.4×10^1,15 μm gap, drop casting and 2.8×10^3, 10 μm gap, slot-die). Optimizing only the inter-electrode gap gives over 20 times improvement in I_{UV}/I_{Dark} ratio (Table S3, supporting information and Fig. 7).

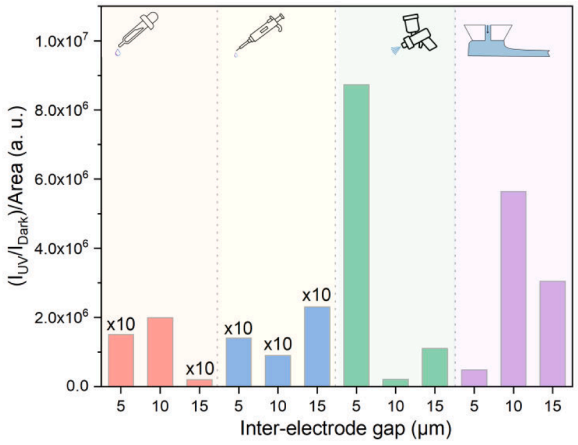

Fig. 7. I_{UV}/I_{Dark} ratio normalized to the unit area (1 cm^2) for different inter-electrode gap UV sensors prepared by coating methods: drop casting (marked red), microdrop casting (marked blue), spray coating (marked green), slot-die (marked purple).

The critical role in ZnO UV photodetectors is played by oxygen chemisorption on the surface [49]. In the dark, oxygen adsorbs on the surface capturing free electrons from ZnO and inducing an electron depleted layer with low conductivity. The thickness of such the depleted layer equals to Debye length [10]. Under UV illumination, photo-generated holes migrate to the surface and discharge the adsorbed oxygen through surface recombination. The photo-generated electrons also significantly increase the conductivity [50].

The crucial parameter is the diameter of ZnO-T leg, which ideally should be double of the Debye length. The photoresponse of wide bandgap photodetector is dependent mainly on the ratio between the Debye length and the nanoparticle diameter. If the diameter is larger than twice Debye length, then under UV illumination the inner part of the nanoparticle stays undepleted, a conduction channel is formed leading to higher dark current. If the diameter is decreased, the contribution of the depletion layer domains increases, to the total film conductivity resulting in higher photoresponse [51]. Debye length at room temperature for ZnO is ≈19 nm [10], which means that highest photoresponse can be expected for the ZnO nanoparticle diameters larger than 38 nm. ZnO-Ts used in this work have an average diameter of about 50 nm, which might explain the low dark current and high photoresponse in our measurements.

It should be also kept in mind, that ZnO-T leg length is at least an order of magnitude shorter than inter-electrode gap, so multiple leg to leg contacts is involved in the conduction path from one electrode to the other. Leg to leg contacts can cause higher sensitivity, as it involves the tunneling though depletion layer [52], however long conduction path with many contacts can lower both the dark and photo current due to high resistance.

The photoresponse can be also attributed to the morphology of the coating, especially aggregations. A high porosity of the coating facilitates the penetration of oxygen into the lower layers, involving the whole coating in the sensing mechanism. In the same way the UV penetration can be hindered by the dense upper layers [10]. Based on morphology to photoresponse relation can connect the lowest photoresponse of microdrop casting coatings to multiple coffee-rings, appearing on the inter-electrode gap. The spray and slot-die coatings show best photoresponse due to uniform distribution of ZnO-Ts on the surface.

The influence of different coating methods on photoresponse can be explained by the microstructure formed after deposition. Drop and

Table 1
Overview of reported state-of-the-art ZnO photodetectors properties with respect to this work.

Photodetector	Bias (V)	UV light intensity ($mWcm^{-2}$)	Wavelength (nm)	Area (mm × mm)	Rise time (s)	Decay time (s)	I_{Photo}/I_{Dark} ratio	I_{Photo}/I_{Dark} ratio per area	Ref.
ZnO-T (Spray coating)	−5	0.31	365	0.005 × 5	6.4	4.0	2.2×10^3	8.7×10^6	This Work
ZnO-T (Slot-die coating)	−5	0.31	365	0.01 × 5	1.4	0.8	2.8×10^3	5.6×10^6	This Work
ZnO ultraporous nanoparticle networks	5	0.02	370	7 × 5	≈250	≈150	7.2×10^4	2×10^5	[10]
ZnO@A-SWNT film	2	0.47	365	1 × 3	11.3	5.97	$\sim 10^4$	0.3×10^6	[54]
ZnO nanowire	1	1.3	360	10 × 10	40	300	10^3	10^3	[30]
ZnO film	1	0.1	365	22 × 17	62.6	30.1	1.3×10^6	3.48×10^5	[19]

Our work shows the importance of coating morphology and inter-electrode gap optimization. We demonstrate that even with the same optimized ZnO-T nanostructures I_{UV}/I_{Dark} ratio (per 1 cm^2) can be improved by 437-fold.

microdrop casting methods show a descending order of UV current (I_{UV}) with the increasing length of the inter-electrode gap. This can be connected to the increasing length of the conduction path and therefore increasing amount ZnO-T leg-leg contacts and consequently higher contact resistance [53]. The spray and slot-die coating methods do not show a direct I_{UV} dependance on the inter-electrode gap, i.e., slot-die coated sensor shows the highest I_{UV} value for 10 μm inter-electrode gap, while a spray coating for the 15 μm, which can be both explained by the ZnO-T formed microstructure in the coating. The spray and slot-die coating methods' photoresponse inconsistency with gap size could be caused by stochastic distribution of the spherical and hillock nanoparticle aggregations on the surface. Since the size of such aggregations is in the order of the inter-electrode gaps, there is a probability of such aggregation formation on the gap, affecting the overall sensing performance or even short-cutting or creating alternative conduction paths through the gap.

Hillocks induced by slot-die coating can be regarded as thickening of the ZnO-T film. In case some hillocks appear over the inter-electrode gap, such places have thicker ZnO-T film, therefore more ZnO-Ts are on the conductance path. This might explain that slot-die coated sensors due to thicker patches have enhanced photoresponse for 15 μm inter-electrode gap, while more evenly distributed spray coated sensors demonstrated best photoresponse at the shortest inter-electrode gaps of 5 μm. It should be noted that slot-die coated sensor demonstrated higher I_{UV}/I_{Dark} ratio, however normalized per unit area spray coated sensor became 1.6 times higher. This can be explained by the shadowing and scattering effects of the thicker nanoparticle films [10].

Miniaturization is the prevailing trend in microelectronics, therefore, it is important to evaluate the sensor performance in connection to the occupied surface area. To evaluate the practical efficiency of our sensors prepared by different deposition methods and to compare them to the state-of-the-art UV sensors we normalized the I_{UV}/I_{Dark} ratio per unit area of 1 cm^2 (Table 1). Slot-die coating and spray coating showed the best performance per unit area, whereas the 5 μm gap spray-coated sensor showed the record-breaking I_{UV}/I_{Dark} ratio (per 1 cm^2) of 8.73 × 10^6. To the best of our knowledge the highest I_{UV}/I_{Dark} ratio for UV sensor is 7.2 × 10^4 [10] and 10^4 [54], converted per unit area these sensors are exceeded at least 26-fold by slot-die coated sensor, prepared in this work.

Conclusions

We demonstrated the importance of coating morphology and inter-electrode gap optimization for UV photodetector response enhancement. The same ZnO-T nanostructure-based UV sensor I_{UV}/I_{Dark} ratio was improved 437-fold, by optimizing the coating method and inter-electrode gap. The record I_{UV}/I_{Dark} ratio per 1 cm^2 value of 8.73 × 10^6 was obtained by spray coated sensor with the 5 μm inter-electrode gap. Highest I_{UV}/I_{Dark} ratio without normalization per unit area was demonstrated by slot-die coated sensor with 10 μm gap. The fastest rise time 0.78 s and fastest decay time 0.94 s were obtained by slot-die coated sensors with the inter-electrode gap of 5 μm and 15 μm, respectively. High photoresponse of ZnO-Ts is expected, as the mean leg diameter is close to double of the Debye length. The inter-electrode gap size influences the photoresponse due to multiple ZnO-T leg-leg contacts on the conduction path, therefore optimization involves the interplay between higher contact resistance and higher sensitivity due to tunneling though depletion zone on leg-leg contacts. The influence of different coating methods on photoresponse can be explained by the processes taking place on the microstructure formed after deposition. The new direction for ZnO or other semiconductor nanoparticle based chemoresistive sensor improvement can be envisioned.

Declaration of Competing Interest

The authors declare that they have no known competing financial interests or personal relationships that could have appeared to influence the work reported in this paper.

Data availability

Data will be made available on request.

Acknowledgments

This research was funded by a grant (proposal No. P-MIP-21-145, contract No. S-MIP-21-54) from the Research Council of Lithuania, project title "Room temperature selective gas sensing with self-assembled monolayers on ZnO nanowire networks".

Supplementary materials

Supplementary material associated with this article can be found, in the online version, at doi:10.1016/j.jpap.2023.100171.

References

[1] P.M. Faia, C.S. Furtado, Effect of composition on electrical response to humidity of TiO2:ZnO sensors investigated by impedance spectroscopy, Sens. Actuators B 181 (2013) 720–729, https://doi.org/10.1016/j.snb.2013.02.027.
[2] M. Al-Fandi, et al., A prototype ultraviolet light sensor based on ZnO nanoparticles/graphene oxide nanocomposite using low temperature hydrothermal method, IOP Conf. Ser. Mater. Sci. Eng. 92 (2015), 012009, https://doi.org/10.1088/1757-899x/92/1/012009.
[3] S.-.P. Chang, et al., A ZnO nanowire-based humidity sensor, Superlattices Microstruct. 47 (6) (2010) 772–778, https://doi.org/10.1016/j.spmi.2010.03.006.
[4] Y.K. Mishra, R. Adelung, ZnO tetrapod materials for functional applications, Mater. Today 21 (6) (2018) 631–651, https://doi.org/10.1016/j.mattod.2017.11.003.
[5] S. Rackauskas, et al., A Novel Method for Continuous Synthesis of ZnO Tetrapods, J. Phys. Chem. C 119 (28) (2015) 16366–16373, https://doi.org/10.1021/acs.jpcc.5b03702.
[6] S. Rackauskas, N. Barbero, C. Barolo, G. Viscardi, ZnO nanowire application in chemoresistive sensing: a review, Nanomaterials 7 (11) (2017) 381, https://doi.org/10.3390/nano7110381.
[7] M.C. Newton, P.A. Warburton, ZnO tetrapod nanocrystals, Mater. Today 10 (5) (2007) 50–54, https://doi.org/10.1016/S1369-7021(07)70079-2.

[8] Y.K. Mishra, R. Adelung, ZnO tetrapod materials for functional applications, Mater. Today 21 (6) (2018) 631–651, https://doi.org/10.1016/j.mattod.2017.11.003.

[9] H. Zheng, et al., ZnO nanorods array as light absorption antenna for high-gain UV photodetectors, J. Alloys Compd. 812 (2020), 152158, https://doi.org/10.1016/j.jallcom.2019.152158.

[10] N. Nasiri, R. Bo, F. Wang, L. Fu, A. Tricoli, Ultraporous electron-depleted ZnO nanoparticle networks for highly sensitive portable visible-blind UV photodetectors, Adv. Mater. 27 (29) (2015) 4336–4343, https://doi.org/10.1002/adma.201501517.

[11] D. Gedamu, et al., Rapid fabrication technique for interpenetrated ZnO nanotetrapod networks for fast UV sensors, Adv. Mater. 26 (10) (2014) 1541–1550, https://doi.org/10.1002/adma.201304363.

[12] W. Gao, Z. Li, ZnO thin films produced by magnetron sputtering, Ceram. Int. 30 (7) (2004) 1155–1159, https://doi.org/10.1016/j.ceramint.2003.12.197.

[13] S. Marouf, et al., Low-temperature spray-coating of high-performing ZnO:Al films for transparent electronics, J. Anal. Appl. Pyrolysis 127 (2017) 299–308, https://doi.org/10.1016/j.jaap.2017.07.021.

[14] S. Jeevan, M. Venkatachalam, M. Manickam, ZNO thin film prepared by dip coating technique for gas sensing application, Int. J. Res. Appl. Sci. Eng. Technol. V (2017) 417–419, https://doi.org/10.22214/ijraset.2017.10061.

[15] W. Shen, Y. Zhao, C. Zhang, The preparation of ZnO based gas-sensing thin films by ink-jet printing method, Thin. Solid. Films 483 (1) (2005) 382–387, https://doi.org/10.1016/j.tsf.2005.01.015.

[16] S.A. Kamaruddin, K.-.Y. Chan, H.-.K. Yow, M. Zainizan Sahdan, H. Saim, D. Knipp, Zinc oxide films prepared by sol–gel spin coating technique, Appl. Phys. A 104 (1) (2011) 263–268, https://doi.org/10.1007/s00339-010-6121-2.

[17] S.M. Mane, et al., NO2 sensing properties of 3D flower-like ZnO nanostructure decorated with thin porous petals synthesized using a simple sol–gel drop-casting method, Appl. Phys. A 127 (1) (2021) 13, https://doi.org/10.1007/s00339-020-04152-7.

[18] D.J. Winarski, et al., Photoconductive ZnO films printed on flexible substrates by inkjet and aerosol jet techniques, J. Electron. Mater. 47 (2) (2018) 949–954, https://doi.org/10.1007/s11664-017-5903-0.

[19] Q. Xu, et al., Flexible self-powered ZnO Film UV sensor with a high response, ACS Appl. Mater. Interfaces 11 (29) (2019) 26127–26133, https://doi.org/10.1021/acsami.9b09264.

[20] R.A. Sabty-Daily, W.C. Hinds, J.R. Froines, Size distribution of chromate paint aerosol generated in a bench-scale spray booth, Ann. Occup. Hyg. 49 (1) (2005) 33–45, https://doi.org/10.1093/annhyg/meh080.

[21] S. Marouf et al., "Low-temperature spray-coating of high-performing ZnO:Al films for transparent electronics," J. Anal. Appl. Pyrolysis, vol. 127, pp. 299–308, 2017, doi: 10.1016/j.jaap.2017.07.021.

[22] O. Kwon, Y. Choi, E. Choi, M. Kim, Y.C. Woo, D.W. Kim, Fabrication techniques for graphene oxide-based molecular separation membranes: towards industrial application, Nanomaterials 11 (3) (2021) 757, https://doi.org/10.3390/nano11030757.

[23] J.R. Anusha, et al., Simple fabrication of ZnO/Pt/chitosan electrode for enzymatic glucose biosensor, Sens. Actuators B 202 (2014) 827–833, https://doi.org/10.1016/j.snb.2014.06.024.

[24] R.D. Deegan, O. Bakajin, T.F. Dupont, G. Huber, S.R. Nagel, T.A. Witten, Contact line deposits in an evaporating drop, Phys. Rev. E 62 (1) (2000) 756–765, https://doi.org/10.1103/PhysRevE.62.756.

[25] D. Orejon, K. Sefiane, M.E.R. Shanahan, Stick–slip of evaporating droplets: substrate hydrophobicity and nanoparticle concentration, Langmuir 27 (21) (2011) 12834–12843, https://doi.org/10.1021/la2026736.

[26] R. Bhardwaj, X. Fang, P. Somasundaran, D. Attinger, Self-assembly of colloidal particles from evaporating droplets: role of DLVO interactions and proposition of a phase diagram, Langmuir 26 (11) (2010) 7833–7842, https://doi.org/10.1021/la9047227.

[27] M. Parsa, S. Harmand, K. Sefiane, Mechanisms of pattern formation from dried sessile drops, Adv. Colloid Interface Sci. 254 (2018) 22–47, https://doi.org/10.1016/j.cis.2018.03.007.

[28] X. Shen, C.-.M. Ho, T.-.S. Wong, Minimal size of coffee ring structure, J. Phys. Chem. B 114 (16) (2010) 5269–5274, https://doi.org/10.1021/jp912190v.

[29] J.H. Jun, H. Seong, K. Cho, B.-.M. Moon, S. Kim, Ultraviolet photodetectors based on ZnO nanoparticles, Ceram. Int. 35 (7) (2009) 2797–2801, https://doi.org/10.1016/j.ceramint.2009.03.032.

[30] A. Manekkathodi, M.-.Y. Lu, C.W. Wang, L.-.J. Chen, Direct growth of aligned zinc oxide nanorods on paper substrates for low-cost flexible electronics, Adv. Mater. 22 (36) (2010) 4059–4063, https://doi.org/10.1002/adma.201001289.

[31] M. Kumar, H. Jeong, D. Lee, UV photodetector with ZnO nanoflowers as an active layer and a network of Ag nanowires as transparent electrodes, Superlattices Microstruct. 126 (2019) 132–138, https://doi.org/10.1016/j.spmi.2018.12.004.

[32] Y. Wang, et al., Electrical properties of fluorine-doped ZnO nanowires formed by biased plasma treatment, Physica E 99 (2018) 254–260, https://doi.org/10.1016/j.physe.2018.01.028.

[33] A.M. Nahhas, Review of recent advances of ZnO nanowires based sensors, Am. J. Nanomater. 8 (1) (2020) 18–32, https://doi.org/10.12691/ajn-8-1-3.

[34] M. Lord, A.S. Walton, T.G. Maffeis, M.B. Ward, P. Davies, S.P. Wilks, ZnO nanowires with Au contacts characterised in the as-grown real device configuration using a local multi-probe method, Nanotechnology 25 (42) (2014), 425706, https://doi.org/10.1088/0957-4484/25/42/425706.

[35] S.-.H. Kim, H.-.K. Kim, S.-.W. Jeong, T.-.Y. Seong, Characteristics of Pt Schottky contacts on hydrogen peroxide-treated n-type ZnO(0001) layers, Superlattices Microstruct. 39 (1) (2006) 211–217, https://doi.org/10.1016/j.spmi.2005.08.044.

[36] V. Galstyan, E. Comini, I. Kholmanov, G. Faglia, G. Sberveglieri, Reduced graphene oxide/ZnO nanocomposite for application in chemical gas sensors, RSC Adv. 6 (41) (2016) 34225–34232, https://doi.org/10.1039/C6RA01913G.

[37] R. Saad, et al., Fabrication of ZnO/CNTs for application in CO2 sensor at room temperature, Nanomaterials 11 (11) (2021), https://doi.org/10.3390/nano11113087.

[38] M.-.Y. Lu, M.-.P. Lu, S.-.J. You, C.-.W. Chen, Y.-.J. Wang, Quantifying the barrier lowering of ZnO Schottky nanodevices under UV light, Sci. Rep. 5 (1) (2015) 15123, https://doi.org/10.1038/srep15123.

[39] J.D. Hwang, F.H. Wang, C.Y. Kung, M.C. Chan, Using the surface plasmon resonance of au nanoparticles to enhance ultraviolet response of ZnO nanorods-based Schottky-Barrier photodetectors, IEEE Trans. Nanotechnol. 14 (2) (2015) 318–321, https://doi.org/10.1109/TNANO.2015.2393877.

[40] S. Rackauskas, et al., A novel method for continuous synthesis of ZnO tetrapods, J. Phys. Chem. C 119 (28) (2015) 16366–16373, https://doi.org/10.1021/acs.jpcc.5b03702.

[41] J.S. Galsin, Chapter 1 - Crystal structure of solids, in: J.S. Galsin (Ed.), Solid State Physics, Academic Press, 2019, pp. 1–36, https://doi.org/10.1016/B978-0-12-817103-5.00001-3.

[42] P. Scherrer, Bestimmung der Größe und der inneren Struktur von Kolloidteilchen mittels Röntgenstrahlen, Nachrichten von der Gesellschaft der Wissenschaften zu Göttingen, Mathematisch-Physikalische Klasse 1918 (1918) 98–100 [Online]. Available, http://eudml.org/doc/59018.

[43] A. Sulciute, et al., ZnO Nanostructures application in electrochemistry: influence of morphology, J. Phys. Chem. C 125 (2) (2021) 1472–1482, https://doi.org/10.1021/acs.jpcc.0c08459.

[44] K. Zak, M.E. Abrishami, W.H. Abd. Majid, R. Yousefi, S.M. Hosseini, Effects of annealing temperature on some structural and optical properties of ZnO nanoparticles prepared by a modified sol–gel combustion method, Ceram. Int. 37 (1) (2011) 393–398, https://doi.org/10.1016/j.ceramint.2010.08.017.

[45] D.Jang Seo, J. Chae, S. Shin, Altering the coffee-ring effect by adding a surfactant-like viscous polymer solution, Sci. Rep. 7 (1) (2017) 500, https://doi.org/10.1038/s41598-017-00497-x.

[46] H. Hu, R.G. Larson, Marangoni effect reverses coffee-ring depositions, J. Phys. Chem. B 110 (14) (2006) 7090–7094, https://doi.org/10.1021/jp0609232.

[47] J. Fischer, Particle convection in an evaporating colloidal droplet, Langmuir 18 (1) (2002) 60–67, https://doi.org/10.1021/la015518a.

[48] Y.K. Mishra, et al., Direct growth of freestanding ZnO tetrapod networks for multifunctional applications in photocatalysis, UV photodetection, and gas sensing, ACS Appl. Mater. Interfaces 7 (26) (2015) 14303–14316, https://doi.org/10.1021/acsami.5b02816.

[49] Q.H. Li, T. Gao, Y.G. Wang, T.H. Wang, Adsorption and desorption of oxygen probed from ZnO nanowire films by photocurrent measurements, Appl. Phys. Lett. 86 (12) (2005), 123117, https://doi.org/10.1063/1.1883711.

[50] H. Kind, H. Yan, B. Messer, M. Law, P. Yang, Nanowire ultraviolet photodetectors and optical switches, Adv. Mater. 14 (2) (2002) 158–160, https://doi.org/10.1002/1521-4095(20020116)14:2<158::AID-ADMA158>3.0.CO;2-W.

[51] A. Tricoli, M. Graf, S.E. Pratsinis, Optimal doping for enhanced SnO2 sensitivity and thermal stability, Adv. Funct. Mater. 18 (13) (2008) 1969–1976, https://doi.org/10.1002/adfm.200700784.

[52] S. Rackauskas, et al., Synthesis of ZnO tetrapods for flexible and transparent UV sensors, Nanotechnology 23 (9) (2012) 95502, https://doi.org/10.1088/0957-4484/23/9/095502.

[53] G. Modi, Zinc oxide tetrapod: a morphology with multifunctional applications, Adv. Nat. Sci. 6 (3) (2015), 033002, https://doi.org/10.1088/2043-6262/6/3/033002.

[54] M.-.S. Choi, T. Park, W.-.J. Kim, J. Hur, High-performance ultraviolet photodetector based on a zinc oxide nanoparticle@single-walled carbon nanotube heterojunction hybrid film, Nanomaterials 10 (2) (2020) 395, https://doi.org/10.3390/nano10020395.